THE JOURNAL OF BIOLOGICAL CHEMISTRY VOL. 286, NO. 2, pp. 1260–1268, January 14, 2011

Nature of the Ferryl Heme in Compounds I and II*

Received for publication, October 4, 2010, and in revised form, November 4, 2010 Published, JBC Papers in Press, November 8, 2010, DOI 10.1074/jbc.M110.183483

Andrea Gumiero[‡], Clive L. Metcalfe[‡], Arwen R. Pearson[§], Emma Lloyd Raven[‡1], and Peter C. E. Moody[¶2]

From the [‡]Department of Chemistry, Henry Wellcome Building, University of Leicester, University Road, Leicester LE1 7RH, the [§]Astbury Centre for Structural Molecular Biology, Institute for Molecular and Cellular Biology, Astbury Building, University of Leeds, Leeds LS2 9JT, and the [¶]Department of Biochemistry and Henry Wellcome Laboratories for Structural Biology, Henry Wellcome Building, University of Leicester, Lancaster Road, Leicester LE1 9HN, United Kingdom

Heme enzymes are ubiquitous in biology and catalyze a vast array of biological redox processes. The formation of high valent ferryl intermediates of the heme iron (known as Compounds I and Compound II) is implicated for a number of catalytic heme enzymes, but these species are formed only transiently and thus have proved somewhat elusive. In consequence, there has been conflicting evidence as to the nature of these ferryl intermediates in a number of different heme enzymes, in particular the precise nature of the bond between the heme iron and the bound oxygen atom. In this work, we present high resolution crystal structures of both Compound I and Compound II intermediates in two different heme peroxidase enzymes, cytochrome *c* peroxidase and ascorbate peroxidase, allowing direct and accurate comparison of the bonding interactions in the different intermediates. A consistent picture emerges across all structures, showing lengthening of the ferryl oxygen bond (and presumed protonation) on reduction of Compound I to Compound II. These data clarify long standing inconsistencies on the nature of the ferryl heme species in these intermediates.

Aerobic organisms have evolved to utilize the intrinsic oxidizing power of dioxygen. In a large majority of cases, this so-called "activation" of oxygen is catalyzed by a metal center (usually iron or copper) buried within a protein structure (1). The large and biologically diverse family of catalytic iron-containing heme proteins is one such group of enzymes capable of oxygen activation. Oxygen activation by heme is achieved through formation of highly oxidized iron intermediates, which are known as Compound I and Compound II. Compound I is formally oxidized by two (electron) equivalents above the ferric heme resting state; Compound II is the reduced form of Compound I and thus oxidized by only one equivalent. Nature uses these intermediates for a large number of quite different, and sometimes difficult, biological oxidations. The most well cited examples are in the cytochrome P450s, nitric oxide synthases, cytochrome *c* oxidases, and heme peroxidases (2–5). It appears that there are two possible routes for formation of Compound I, a direct reaction with hydrogen peroxide (*e.g.* the peroxidase enzymes) or reaction with dioxygen followed by a further reduction of the heme by a suitable reductase (*e.g.* the P450s, NO synthase (Scheme 1)). However, the shared heme structure used in all of these enzymes, together with the similarity of their reactions with dioxygen or dioxygen derivatives, make it highly likely that these intermediates and their mechanisms of formation are a defining feature across the family.

It is no surprise, therefore, that elucidation of the structure of these heme intermediates has provided an important focus and is the source of continuing high profile comment and debate (see for example Ref. 6). However, the quest to unravel the structure and properties of Compounds I and II has not been at all straightforward, not least because of the experimental difficulties associated with observing such metastable species. A key challenge has been to clarify the precise nature of the ferryl heme species as the literature reports conflicting bond lengths measured for the Compound I or Compound II intermediates in different proteins. The main experimental approaches have used EXAFS[3] data and crystallography, but an inconsistent picture emerges (see Ref. 7 for a recent summary). This has made it difficult to determine the bonding interactions with confidence (Fe(IV)=O *versus* Fe(IV)–OH, the latter being a longer bond). This is made yet more complicated by the fact that many previous crystallographic studies are likely to have been affected by photoelectron reduction in the x-ray beam so that deduced structures are unlikely to represent "pure" species. Although the effect of x-ray photoreduction on the reaction intermediates has been explored in detail for horseradish peroxidase (HRP) (8), a precise structural characterization of these intermediates has not been achieved in any other enzymes.

In this work, we present crystal structures of both the Compound I and the Compound II intermediates in two different peroxidase enzymes, cytochrome *c* peroxidase (C*c*P) and the closely related ascorbate peroxidase (APX). The structures provide reliable measurements of bond distances and in both cases indicate a lengthening of the bond on reduction that is presumed to be coupled to protonation. The likely mechanisms of proton delivery to the transient ferryl heme are also revealed. The information is relevant to our understanding of

* This work was supported by grants from the Leverhulme Trust (to E. L. R./P. C. E. M.) and ESRF Grants MX1088 and Diamond MX310.

The atomic coordinates and structure factors (codes 2xih, 2xi6, 2xif, 2xj6, 2xil, 2xj5, and 2xj8) have been deposited in the Protein Data Bank, Research Collaboratory for Structural Bioinformatics, Rutgers University, New Brunswick, NJ (http://www.rcsb.org/).

[1] To whom correspondence may be addressed. Tel.: 44-116-2297047; Fax: 44-116-252-3789; E-mail: emma.raven@le.ac.uk.

[2] To whom correspondence may be addressed. Tel.: 44-116-2297097; Fax: 44-116-252-7084; E-mail: peter.moody@le.ac.uk.

[3] The abbreviations used are: EXAFS, extended x-ray absorption fine structure; APX, ascorbate peroxidase; C*c*P, cytochrome *c* peroxidase; sh, shoulder; ESU, estimated standard uncertainty; MGy, megagrays.

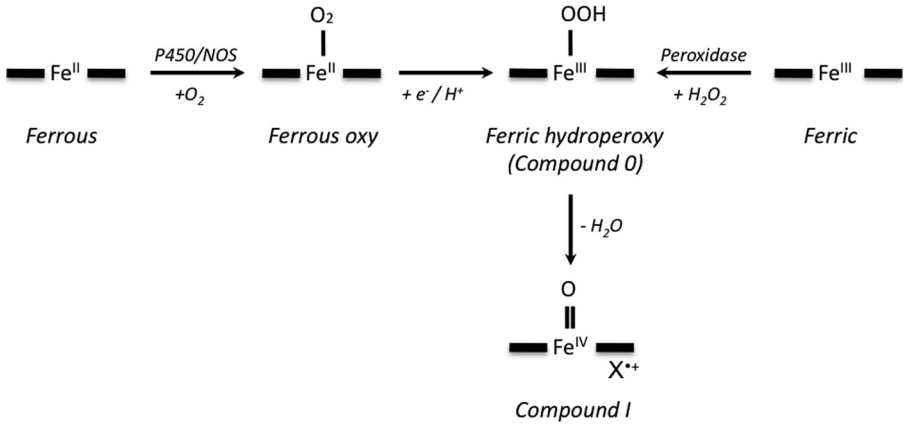

SCHEME 1. **Different routes for oxygen activation by heme enzymes.** The reaction using dioxygen (in the P450s and NO synthases) or hydrogen peroxide (in the peroxidases) as a route to the activated Compound I intermediate is shown. $X^{\bullet+}$ represents either a porphyrin π-cation radical or a tryptophan radical.

oxygen activation across the family of heme enzymes and is discussed in this more general context.

EXPERIMENTAL PROCEDURES

Protein Purification and Expression—The MKT variant of C*c*P (9) was prepared as previously described but cloned into the expression plasmid pLEICS-03 carrying kanamycin resistance and a tobacco etch virus-cleavable N-terminal His tag sequence and expressed in BL21 DE3 Gold (Fisher Scientific). Expression and purification of APX were carried out as previously described (10, 11).

Both C*c*P and APX were crystallized as previously described (12, 13). C*c*P crystals were grown in 50 mM potassium phosphate, pH 6.0, containing (±)-2-methyl-2,4-pentanediol (30% v/v), and APX crystals were prepared from Li_2SO_4 (2.25 M) containing HEPES (0.1 M), pH 8.3. Compound I of C*c*P was formed by soaking crystals of ferric enzyme in freshly prepared H_2O_2 (20 mM) for 5 min, and crystals were then flash-frozen at 100 K. Compounds II and III of APX were prepared by soaking the ferric enzyme in H_2O_2 (200 μM) for 5 min or H_2O_2 (20 mM) for 5 min, respectively, and frozen as above. Crystals were stored in liquid nitrogen.

Monitoring of Photoreduction—Changes in UV-visible absorbance spectra during x-ray exposure were monitored at the European Synchrotron Radiation Facility (ESRF) ID14-2 using an on-line spectrophotometer (OCEAN OPTICS DH 2000 light source and HR 2000 detector). UV-visible spectra of exposed crystals used to solve the structure of C*c*P Compound II, APX Compound I, ferrous C*c*P, and APX were measured using a 4DX single crystal microspectrophotometer with a Shamrock SR-163 spectrograph and Newton CCD camera (Andor Technology).

Crystallographic Data Collection and Analysis—For the structure of C*c*P intermediates, x-ray diffraction data were collected in-house at 100 K using CuKα radiation (λ = 1.5418 Å) from a Rigaku RU2HB x-ray generator with a copper anode and Xenocs multilayer optics and measured with an R-AXIS IV detector. For APX, diffraction data were collected on beam line I04 (wavelength λ = 0.6 Å) at Diamond Light Source, Harwell, UK using an ADSC Q315 CCD detector, at 100 K. C*c*P data were indexed, integrated, merged, and scaled, respectively, using MOSFLM, SORTMTZ, and SCALA as part of the CCP4 suite (14, 15); APX data were integrated, merged, and scaled using XDS (16). In all cases, 5% of the data were flagged for the calculation of R_{free} and excluded from subsequent refinement. Data collection statistics are shown in Table 1.

Multicrystal Data Analysis—The C*c*P Compound I structure was solved by merging the first 9° of data from 10 different crystals. This corresponds to a maximum absorbed dose of 0.020 MGy (calculated with RADDOSE (17)). We established the amount of data that could be collected from each crystal before the effects of photoreduction showed empirically by truncating the data after various doses. We determined that no detectable change in the observed structure was seen with this (or a lesser) dose but was apparent after a higher dose. The APX Compound II and Compound III structures were solved from three crystals as it was found that by using 0.6 Å radiation, the photoelectron effect is significantly reduced (18), allowing at least 15° to be collected before there was any indication of photoreduction. This corresponds to an absorbed dose of 0.028 MGy (calculated with RADDOSE (17)). Compound I of APX was produced by photoreduction of Compound III (absorbed dose ~0.15 MGy) and verified by UV-visible single crystal spectrophotometry. Diffraction data for Compound I were also obtained from three crystals (using the first 15° after the photoreduction). Compound II of C*c*P was obtained by the photoreduction of Compound I (absorbed dose of ~0.15 MGy) and verified by UV-visible single crystal spectrophotometry. Diffraction data were collected following photoreduction by merging together the first 9° of data from 10 crystals.

Refinement—Crystallographic refinement initially used REFMAC5 (19) from the CCP4 suite (15). The structure of Compound I of C*c*P was refined from the 1.70 Å wild-type C*c*P structure (20) (1ZBY), whereas the structure of Compound II of APX was refined from the 1.45 Å ferric APX structure (13) (1OAG). To ensure the unbiased determination of the iron-oxygen distances, the entire protein structure was refined with the ferryl oxygen atom omitted, and the ferryl oxygen was first fitted to the peak of the $F_o - F_c$ difference

map and refined in real space using Coot (21). The complete models were then refined with SHELX (22), allowing the estimation of individual atomic positional uncertainties (estimated standard uncertainty (ESU)).

RESULTS

We have obtained structures of five reaction intermediates, Compounds I and II for both C*c*P and APX and Compound III (ferrous-oxy) of APX. Compound I of C*c*P and Compounds II and III of APX are isolatable species, and thus we are able to obtain crystals of these directly by reaction with H_2O_2. The structure of C*c*P Compound II was obtained indirectly, by photoreduction of its Compound I; likewise APX Compound I was also obtained indirectly, through photoreduction of Compound III.

CcP Compound I—The structure of the Compound I intermediate of C*c*P has been determined using a multicrystal approach (using only a small percentage of the total data set (8)) to allow the collection of diffraction data before it is affected by photoreduction (Fig. 1*A*). Data and refinement statistics are shown in Table 1. The authenticity of this Compound I species was confirmed using single crystal microspectrophotometry (Fig. 2*A*), which shows the typical Compound I peaks (530, 560, and 632 nm) in the visible region and compares them with previously published spectra (530, 560, and 630^{sh} nm (23)) and with our spectra in solution under the same conditions (*i.e.* using the same ratio of [enzyme]:[H_2O_2] (Fig. 2*A*)). The structure (Fig. 1*A*) reveals an electron density peak for the oxygen atom at 1.63 Å from the iron. This is considerably shorter than previous crystallographic estimates of the Compound I bond length in C*c*P (1.87 Å (24) and 1.7–2.0 Å (25)). The ESU of the iron and oxygen atom positions calculated by full matrix inversion (22) are 0.017 and 0.066 Å, respectively.

The overall structure of Compound I remains unchanged to that of the (nominally) ferric protein (Protein Data Bank (PDB) code 1ZBY). The ferryl iron is positioned about 0.3 Å out of the heme plane in the direction of the distal histidine; the proximal histidine moves with it to bring it closer to the heme plane. This structural shift might be important for stabilization of the high valent heme intermediate. The Nϵ of Trp-51 is seen to be within hydrogen-bonding distance of the ferryl oxygen, as is the Nϵ of Arg-48 (Fig. 1*A*). The side chain of Arg-48 has been observed in two orientations in ferric C*c*P, one with the guanidinium group positioned near the oxygen and above the iron ("in") and the other pointing away ("out") (24–26), but only one of these (in) is seen in the Compound I structure here.

Upon x-ray exposure, photoreduction occurs, leading ultimately to the formation of ferrous heme. After the equivalent of the exposure needed to collect a full set of diffraction data (a dose of ~0.35 MGy), the spectrum corresponds to that of fully reduced, ferrous C*c*P (Fig. 2*A*), but this species first becomes evident after exposure to an absorbed dose of only 0.10–0.15 MGy, suggesting that photoreduction occurs very rapidly in the beam. We have used this photoreduction to obtain a structure for ferrous C*c*P (Fig. 3*A*) (statistics shown in Table 1). In this structure, the bond length to the distal oxygen atom is 2.01 Å, which clearly distinguishes it from that of the Compound I species above (1.63 Å). We note that previously published ferric structures (2CYP and 1ZBY), which have bond lengths of 2.40 and 2.33 Å, respectively, would also be expected to be reduced and thus are probably a mixture of ferrous and ferric states.

APX Compound II—Compound II of APX is also isolatable (27). Its structure was also solved using the multicrystal approach to avoid photoreduction. The corresponding structure of the Compound II derivative of APX is shown in Fig. 1*B*. Microspectrophotometry was used to unambiguously confirm that the crystal was Compound II (Fig. 2*B*). We observe peaks at 531 and 558 nm, which compare well with the spectrum of Compound II obtained in solution by reaction of ferric APX with peroxide under the same conditions (λ_{max} = 530 and 559 nm) and shown for comparison in Fig. 2*B.* In this Compound II crystal structure, the iron-oxygen bond length is 1.84 Å, which is 0.21 Å longer than that for the Compound I derivative of C*c*P above. The ESU of the iron and oxygen positions (22) are 0.015 and 0.088 Å, respectively. When compared with Compound I, this clearly indicates a lengthening of the Fe–O ferryl bond in the Compound II structure. The similarity of the single crystal and solution spectra for Compound II (Fig. 2*B*) and the fact that the bond length for the Compound II species is much shorter than that for either the published ferric APX (2.08 Å) or the ferrous APX (2.20 Å below) give confidence that the assignment of the structure as a Compound II species is correct.

The ferryl iron also moves out of the heme plane by 0.15 Å toward the distal histidine (when compared with the ferric enzyme), and the proximal histidine (His-163) also shifts in the same direction, in the same way as was observed for Compound I of C*c*P above. The side chain of the distal arginine is seen in both the in (as in Compound I) and the out (as in the ferric enzyme) conformations.

As for C*c*P Compound I above, photoreduction of Compound II of APX is observed during exposure to the x-ray beam, leading to the formation of ferrous APX (shown by peaks emerging at 554 nm and a decrease at 534 nm (Fig. 2*B*)) for which we have also obtained a structure (Fig. 3*B*). The distance between the Fe(II) and the oxygen of water is now 2.2 Å, which is much longer than those for any of the Compound I or Compound II species above.

We sought additional structural information on the Compound I and Compound II bond lengths observed above in the corresponding Compound I and Compound II derivatives of APX and C*c*P, respectively. This is described below.

APX Compound I—The Compound I intermediate of APX converts rapidly to Compound II (28), and we are thus unable to isolate this form in the crystal by soaking with peroxide. We can, however, access the Compound I intermediate through the ferrous-oxy (Fe(II)–O_2) species (Compound III), which is used in other catalytic heme enzymes (such as the P450s) as a route to formation of Compound I (Scheme 1). In peroxidases, the ferrous-oxy intermediate can be formed from reaction of Compound II with excess peroxide (8); photoreduction of the ferrous-oxy (Compound III) species thus formed in the crystal converts it to the desired Compound I. The ferrous-oxy species is analogous to the ferric-hydroper-

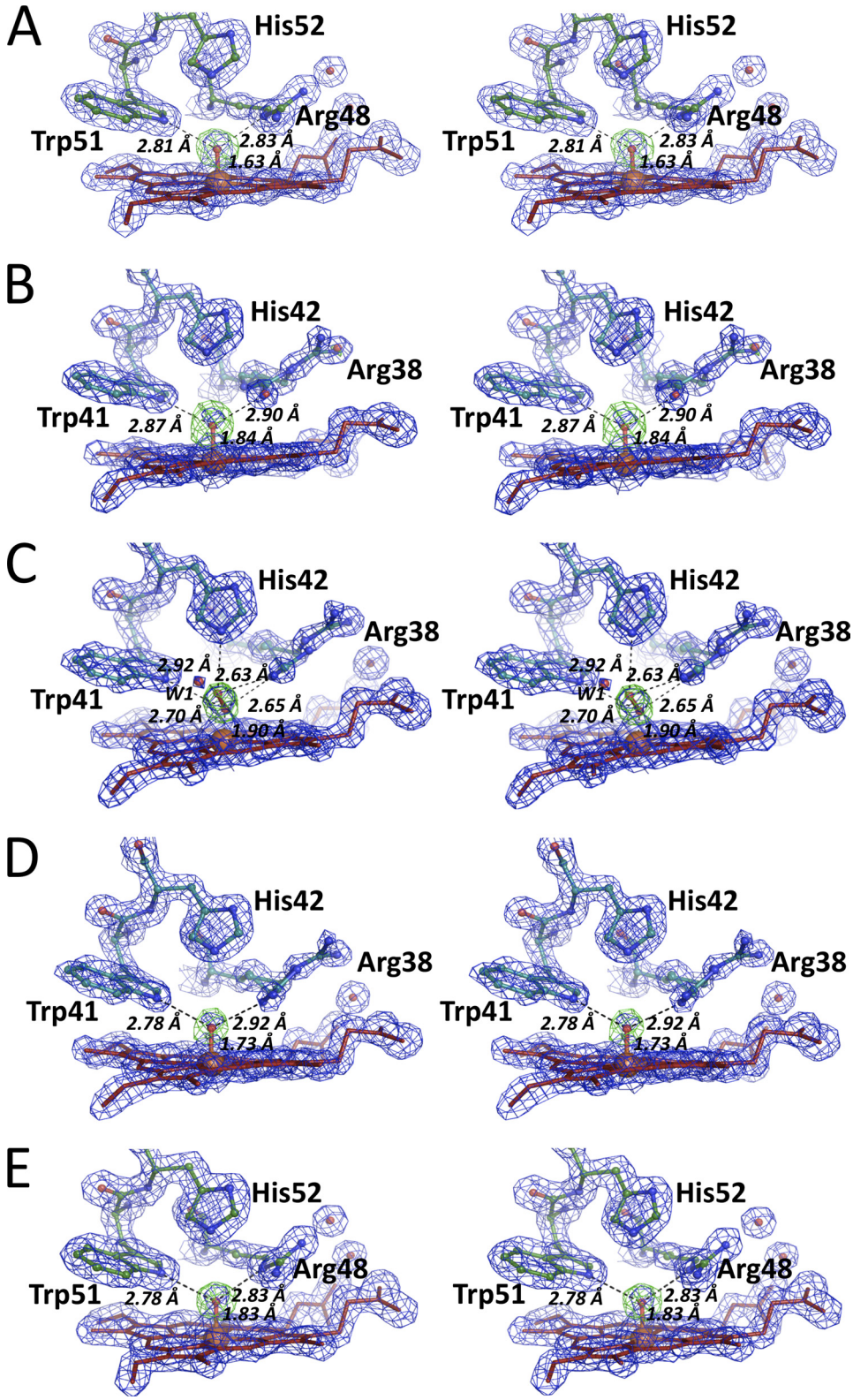

FIGURE 1. **Stereo images of the crystal structures of the ferryl heme intermediates of CcP and APX.** *A–E*, CcP Compound I (*A*). CcP Compound II (*B*), APX Compound III (ferrous-oxy) (*C*), APX Compound I (*D*), APX Compound II (*E*), showing electron density maps calculated with coefficients $2F_o - F_c$ contoured at 2σ in *blue* and the $F_o - F_c$ map (contoured at 4σ, shown in *green*) calculated after refinement omitting the oxygen. Oxygen atoms are shown as *red spheres*, the heme is in *red*, and the iron is shown as an *orange sphere*. Key residues are labeled.

oxide species (sometimes referred to as Compound 0, Fe(III)–OOH) that precedes Compound I and can therefore also report on this transient precursor.

The structure of this ferrous-oxy (Compound III) species is shown in Fig. 1*C*. An electron density peak larger than those observed for the Compound I and Compound II structures is

TABLE 1
Data collection and refinement statistics

	*Cc*P[a]			APX[b]			
	Compound I	Compound II	Ferrous	Compound III	Compound I	Compound II	Ferrous
Data collection[c]							
Space group	$P2_12_12_1$	$P2_12_12_1$	$P2_12_12_1$	$P4_22_12$	$P4_22_12$	$P4_22_12$	$P4_22_12$
Cell dimension *a*, *b*, *c* (Å)	51.04, 75.04, 106.80	51.05, 75.14, 106.92	51.05, 75.19, 106.95	81.97, 81.97, 75.16	82.03, 82.03, 75.23	81.82, 81.82, 75.24	82.24, 82.24, 75.38
Resolution (Å)	1.67 (1.76-1.67)	1.67 (1.76-1.67)	1.69 (1.78-1.69)	1.55 (1.59-1.55)	1.50 (1.54-1.50)	1.65 (1.69-1.65)	1.70 (1.79-1.70)
R_{merge} (%)	6.6 (24.0)	10.5 (26.8)	6.2 (25.5)	6.8 (65.0)	5.1 (33.2)	7.4 (42.3)	10.0 (56.0)
$I/\sigma I$[c]	10.9 (3.8)	5.4 (2.4)	15.8 (4.0)	13.15 (2.0)	14.61 (4.48)	12.1 (2.11)	9.1 (2.4)
Completeness (%)	92 (81)	83.5 (75.8)	99.4 (97.2)	87.9 (69.7)	88.6 (84.7)	99.7 (99.2)	94.5 (88.4)
Multiplicity	2.9 (2.6)	2.1 (2.0)	5.1 (4.5)	3.7 (1.4)	3.0 (3.0)	3.6 (2.6)	3.7 (3.7)
Refinement							
Resolution (Å)	33.11-1.68	33.13-1.68	33.15-1.69	57.96-1.55	27.73-1.50	27.7-1.65	36.79-1.70
No. of reflections	40890	43031	44336	50009	37890	40250	25721
R_{work}/R_{free} (%)	14.4/20.0	14.8/19.9	15.4/19.0	16.0/20.4	14.9/21.5	14.3/19.9	15.2/20.2
Protein	2425	2456	2392	2295	2390	2297	1905
Ligand/ion	97	97	97	57	53	55	1953
Water	685	745	556	479	463	524	434
Overall *B*-factors	16.39	17.62	17.45	17.8	19.32	16.8	15.44
ESU[d] (Å)	0.049	0.052	0.047	0.044	0.040	0.053	0.067
r.m.s.[e] deviations							
Bond lengths (Å)	0.01	0.01	0.01	0.01	0.01	0.02	0.01
Bond angle distances (Å)	0.024	0.025	0.024	0.026	0.024	0.025	0.026

[a] Data collected at home source at wavelength λ = 1.5418 Å merging together the first 9° of data from 10 crystals.
[b] Data were collected at Diamond Light Source beam line IO4 at wavelength λ = 0.6 Å merging the first 15° of data from three crystals. As the atomic cross-section decreases with the wavelength (8), the use of a high energy beam considerably reduced the photoelectric effect and thus decreased the number of crystals needed.
[c] Outer bin data in brackets.
[d] Calculated by the maximum likelihood method (19).
[e] r.m.s., root mean square.

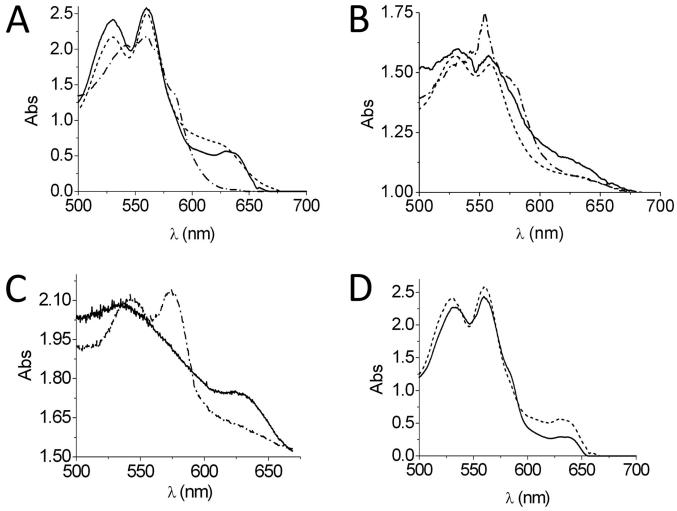

FIGURE 2. **Comparison of UV-visible spectra in solution and from single crystal microspectrophotometry.** *A–D*, comparisons for C*c*P (*A* and *D*) and for APX (*B* and *C*). *A*, the single crystal spectrum of C*c*P Compound I collected before x-ray exposure (*solid line*, maxima: 530, 560, and 632 nm) and after collection of a full dataset (dose > 0.35 Mgy, *dash-dotted line*, maxima: 542, 559, and 585[sh] nm corresponding to reduced heme) when compared with the spectrum of C*c*P Compound I obtained in solution under the same conditions (*dotted line*, maxima: 530, 560, and 630[sh] nm). *Abs*, absorbance. *B*, the spectrum of APX Compound II collected before x-ray exposure (*solid line*, maxima: 531, 558 nm) and after exposure to a dose of 0.3 MGy (*dash-dotted line*, maxima: 537[sh], 554, and 580[sh] nm corresponding to reduced APX (compare 555 and 583 nm (29))) when compared with the solution spectrum of APX Compound II obtained under the same conditions (*dotted line*, maxima: 530, 559 nm (compare 529 and 560 nm (27))). *C*, spectra of APX Compound III (*dash-dotted line*, maxima: 540 and 575 nm) and APX Compound I (*solid line*, maxima 535, 573[sh], and 632 nm) obtained by photoreduction of APX Compound III after exposure to 0.15–0.2 MGy. In all cases, absorbance spectra in solution have been magnified 10 times for comparison. *D*, single crystal spectrum of C*c*P Compound II (*solid line*, maxima: 533, 560, 558[sh], and 633 nm) formed by photoreduction of C*c*P Compound I (*dotted line*) by exposure to a dose of ~0.15–0.2 MGy. Appearance of the shoulder at 585 nm and slight red shift of the β band from 530 to 533 nm indicate the presence minor amounts of ferrous heme formed during photoreduction.

clearly seen and interpreted as a dioxygen species. This is confirmed by single crystal spectrophotometry (peaks at 548 and 575 nm (Fig. 2*C*)). There are hydrogen-bonding interactions from the O^1 of the bound ligand to Nϵ of His-42 (2.92 Å), Nϵ of Trp-41 (2.70 Å), and Nϵ of Arg-38 (2.65 Å). In this case, Arg-38 (equivalent to Arg-48 in C*c*P) is observed occupying both the in and the out positions, and there is a water molecule, seen adjacent to Trp-41 (W1 in Fig. 1*C*), which shifts away from the heme to accommodate the bound O_2 species. Photoreduction leads to cleavage of the O–O bond and the ultimate formation of Compound I (8). We observe that after a dose of ~0.15 MGy, a structure is seen in which only a single atom of oxygen is bound above the iron. Single crystal spectrophotometry (Fig. 2*C*) confirms that this is predominantly Compound I (27), and the structure is shown in Fig. 1*D*. In this structure, the iron-oxygen bond length is 1.73 Å, which is slightly longer than that obtained for the Compound I structure of C*c*P above (most likely because the structure still contains some O_2 bound to the heme (residual ferrous-oxy heme)) but still shorter than previous crystallographic measurements from C*c*P (Table 2). The ESUs of the iron and oxygen positions (22) are 0.016 and 0.09 Å, respectively.

CcP Compound II—As for APX Compound I, Compound II of C*c*P is not stable enough to be trapped and isolated directly in the crystal but can be accessed indirectly through photoreduction of Compound I. The spectrum of C*c*P Compound II is very similar to that of Compound I (the only difference between the two species being that the Trp-191 radical has been reduced in Compound II (23)), which makes unambiguous identification of Compound II in the crystal more difficult, but the intensity of the α- and β-bands decreases on reduction of Compound I to Compound II (23). To obtain a structure for C*c*P Compound II, we have used diffraction data after an exposure of 0.15–0.20 MGy where the α- and β-bands have decreased, but formation of ferrous heme is still negligi-

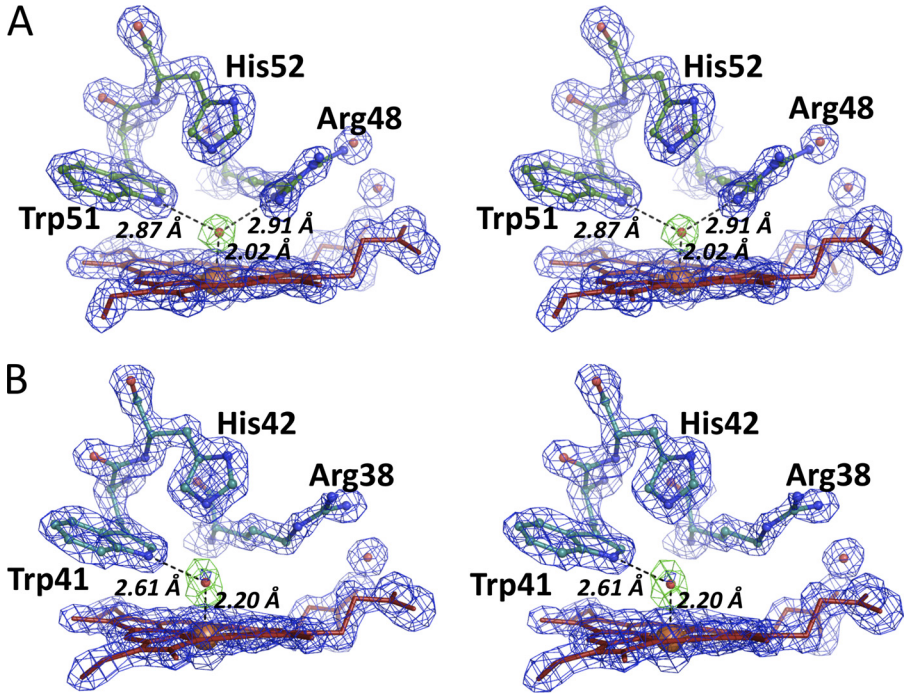

FIGURE 3. **Structures of ferrous heme species.** *A* and *B*, ferrous derivative of C*c*P (*A*) and APX (*B*), showing electron density maps calculated with coefficients $2F_o - F_c$ contoured at 2σ in *blue* and the $F_o - F_c$ map (contoured at 4σ shown in *green*) calculated after refinement omitting the oxygen. Oxygen atoms are shown as *red spheres*, the heme is in *red*, and the iron is shown as an *orange sphere*. Key residues are labeled. For C*c*P, the ESUs of the iron and oxygen atom positions calculated by full matrix inversion are 0.019 and 0.159 Å, respectively; for APX, the corresponding values are 0.023 and 0.170 Å, respectively.

TABLE 2

Summary of Fe–O distances (Å) for Compound I and Compound II intermediates of various heme proteins measured by EXAFS or crystallography

Protein	Compound I	Compound II	Reference
Horseradish peroxidase	1.6[a]	1.6[a]	(41)
	1.64[a]	1.64[a]	(37)
	1.67[a]	1.70[a]	(39)
	1.67[a]	1.93[a]	(38)
	1.7[b]	1.8[a]	(8)
Cytochrome *c* peroxidase[c]	1.67[a]		(35)
	1.87[b]		(24)
	2.0[a,d]		(25)
	1.73[b]		(32)
	1.63[b]	1.83[b]	This work
Ascorbate peroxidase	1.73[b]	1.84[b]	This work
Chloroperoxidase	1.65[a]	1.82[a]	(39, 43)
Myoglobin		1.69[a]	(47)
		1.92[b]	(40, 48)
Cytochrome P450 (CYP 119)		1.82[a]	(30)

[a] From EXAFS.
[b] From x-ray crystallography.
[c] There is an early structure for Compound I of C*c*P (26) but at low resolution (2.5 Å).
[d] In this case, a range of bond lengths is given (1.7–2.0 Å) depending on the refinement.

ble (as monitored by the presence of the characteristic 585 nm peak for the ferrous species (Fig. 2*A*)). Fig. 1*E* shows the structure of the Compound II species thus obtained; single crystal spectra (Fig. 2*D*) confirm the assignment and are in agreement with previous spectra for Compound II (23).[4]

[4] We considered the possibility that the Compound II structures that we present are, in fact, another species such as ferric or ferric-hydroxide, but the microspectrophotometry data are not consistent with such an assignment (ferrous heme is similarly eliminated). The spectrum of ferric APX (29) is easily distinguished from that of Compound II. Our single crystal spectra for C*c*P Compound II also agree with literature values (23) and with the corresponding spectra that we have measured in solution (Fig. 2) and give confidence of assignment.

In this case, the Fe–O distance is observed to clearly increase and is now longer (1.83 Å) than that for both C*c*P Compound I (1.63 Å) and APX Compound I (1.73 Å) above and almost identical to that seen in APX Compound II (1.84 Å). The ESUs of the iron and oxygen positions (22) are 0.017 and 0.065 Å, respectively. Arg-48 mostly remains in the in position, although some positive electron density is observed that is consistent with a low occupancy in the out position.

DISCUSSION

The nature of the Compound I and Compound II intermediates in different heme enzymes has been the subject of intense and sometimes confusing debate (see Ref. 30 for a recent discussion). X-ray crystallographic studies varied in their conclusions on bond length probably because these early structures were photoreduced. A summary of bond lengths from various studies is presented in Table 2.

Here we present the structures of Compound I of C*c*P and Compound II of APX, neither of which is affected by photoreduction. We also present the corresponding (and consistent) structures of Compound I of APX and Compound II of C*c*P. All of the structures obtained here are summarized and compared in Scheme 2. The two proteins share high sequence identity, and their overall structures are very similar (13, 31). This allows a direct and meaningful comparison of the structures of the intermediates in two different proteins. Together with the structures of the ferrous and ferrous-oxy (the latter for APX only) species, this provides a detailed comparative picture of the key redox states (Scheme 2).

Nature of the Ferryl Heme in Compound I—Compound I of C*c*P is stable enough for its structure to be obtained directly. The single crystal spectra and the similarity with the solution

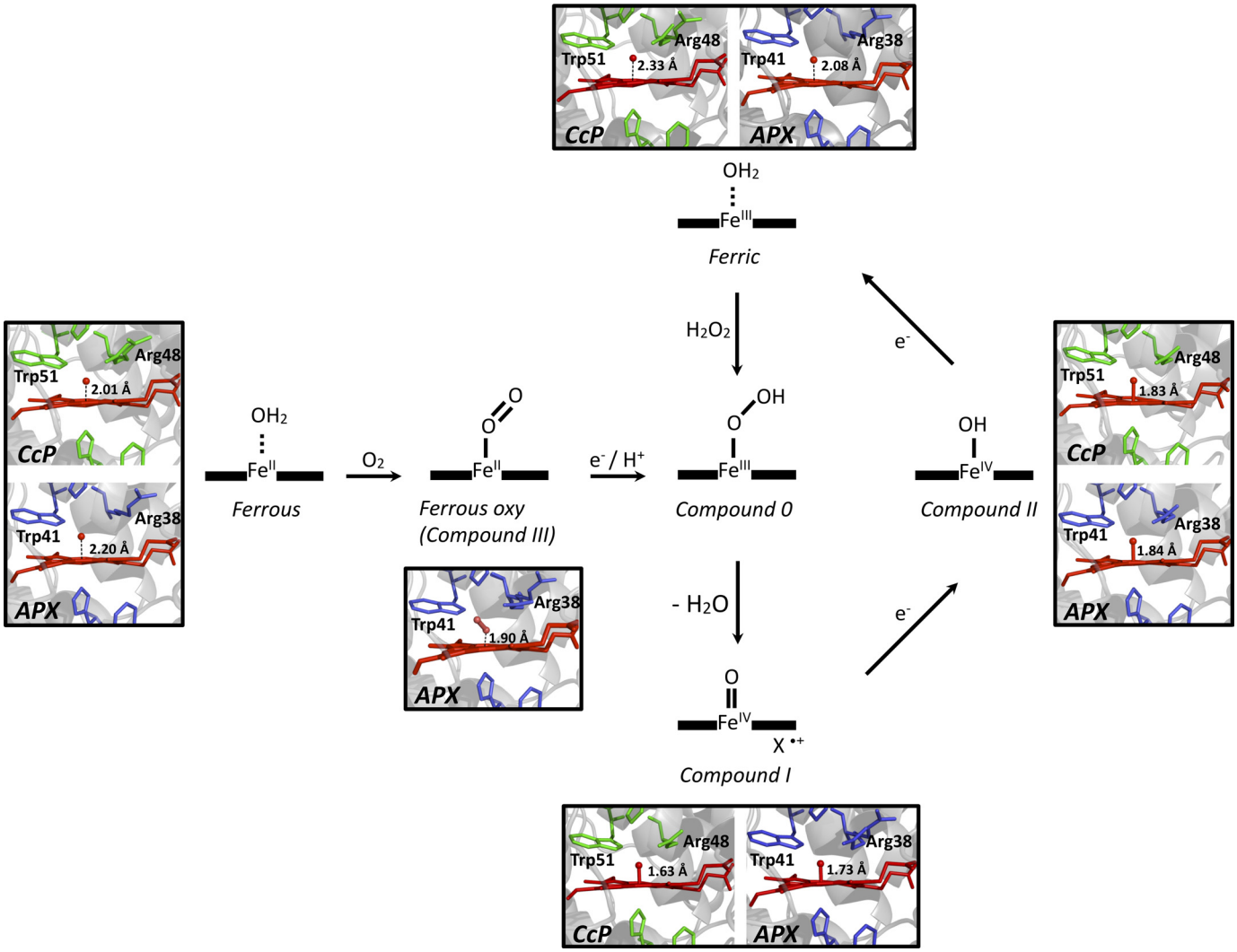

SCHEME 2. **A summary of all structures obtained in this work.** The structures of C*c*P Compound I and APX Compounds II and III were obtained by reaction with hydrogen peroxide; Compound II of C*c*P and Compound I of APX were obtained by photoreduction of Compound I and Compound III, respectively (as described under "Results"). The structures of the ferric C*c*P and APX enzymes are taken from the Protein Data Bank (2ZBY and 1OAG). $X^{\bullet+}$ represents either a porphyrin π-cation radical or a tryptophan radical (APX or *CcP*, respectively).

spectra give a high degree of confidence that the structure corresponds to Compound I. Our crystallographic analyses for this ferryl intermediate in Compound I of C*c*P measures the bond length as 1.63 Å, firmly in the realm of an unprotonated iron–oxo double bond. It is substantially shorter than a previous estimate of 1.87 Å (24), but this structure was affected by photoreduction. This structure can be compared directly with that of APX Compound I. For APX, Compound I is not stable, so its structure necessarily has been obtained indirectly, from photoreduction of the ferrous-oxy intermediate. Nevertheless, the single crystal spectra for the APX Compound I structure are consistent with published data in solution, and the bond lengths in the two Compound I structures are in good agreement; for APX, the bond is slightly longer (1.73 Å) than for C*c*P (1.63 Å), most likely from the presence of residual ferrous-oxy heme (which would increase the apparent bond length). Both bond lengths for Compounds I of C*c*P and APX are shorter than other estimates (24, 25). Both of our Compound I structures show an observed bond length consistent with an unprotonated ferryl (Fe(IV)=O) heme species.

It is worth stating here that the Compound I intermediates of APX and C*c*P are not exactly the same. C*c*P Compound I contains a tryptophan radical (Trp-191) as the site of the second oxidizing equivalent (33). APX contains the equivalent tryptophan residue (Trp-179) but does not use it; instead, APX Compound I contains a porphyrin π-cation radical, and its spectrum thus differs from that of C*c*P Compound I. Our data suggest that this difference in the location of the second oxidizing equivalent does not affect the nature of the ferryl heme species.

Nature of the Ferryl Heme in Compound II—As we discuss below, the nature of the ferryl heme in Compound II has been more controversial. We have presented two Compound II structures. Of them, the APX Compound II structure is the most reliable; APX Compound II is well documented by us (27) and others (34) as an isolatable species. The single crystal spectra that we present for APX Compound II unambiguously

confirm this assignment. For Compound II of APX, the bond length is clearly observed as longer (1.84 Å) than for either of the Compound I structures, consistent with a protonated Fe(IV)–OH (single) bond. This is confirmed in the Compound II structure of C*c*P; in this case, the structure is obtained indirectly (by photoreduction), but the bond also lengthens (to 1.83 Å). Our experiments provide evidence for lengthening of the bond on reduction of Compound I to Compound II in *both* enzymes, and the data are consistent with protonation of the ferryl heme on reduction.

Implications for Other Heme Ferryl Species—Much, but not all, of the confusion in this area has arisen from crystal structures of ferryl heme species that were reduced by the x-ray beam. For C*c*P Compound I, the EXAFS and most of the other data now seem to support an *unprotonated* ferryl-oxy species (32, 35, 36); this is in agreement with our analyses for both C*c*P Compound I and APX Compound I. Compounds I of HRP (8, 37–39) and chloroperoxidase (39) are also not protonated. There seems to be a consensus, therefore, for the Compound I species across several peroxidases.

The picture for Compound II has been even less clear-cut. Much of the information is available for HRP, for which some data favor an unprotonated ferryl unit (7, 36, 37, 39, 41), whereas other work (8, 38) favors a long bond (protonated oxygen). There is only one published structure (8), the reliability of which has been questioned (36, 42, 43). For chloroperoxidase, EXAFS data support a long bond, and thus protonated oxygen, in Compound II (39, 43). Because of this, it has been suggested (42, 44–46) that thiolate ligation is a necessary requirement for protonation of the ferryl heme unit and is thus a unique feature of thiolate-ligated hemes. This would also include the thiolate-ligated P450s, for which there is evidence of a long bond in Compound II (30) but for which characterization of the ferryl heme species has been especially troublesome. The idea that only thiolate-ligated heme proteins are able to form protonated ferryl species is not consistent with our observations for Compounds II of APX and C*c*P, both of which contain imidazole as axial ligand. Our data suggest that the bond lengthening observed in chloroperoxidase (39, 43) and HRP (8) on reduction of Compound I to Compound II is also observed in APX and C*c*P.

Proton Delivery—Any heme enzyme that is using Compound I as an obligate intermediate formally requires two protons for reduction of Compound I back to ferric heme (and concomitant release of the ferryl oxygen atom as water). The source of these protons therefore raises interesting questions. In the case of the peroxidases examined here, the distal arginine appears as a prime suspect. The various structures for both enzymes presented here show different orientations of the distal arginine within the active site (in and out), and in some structures (*e.g.* Compounds I and II of APX), both orientations are observed. For the in orientation, this arginine side chain is close enough to donate a proton to the ferryl oxygen (Fig. 1). The close hydrogen-bonding interaction clearly supports the idea that this distal arginine side chain can potentially provide a proton to the ferryl oxygen of Compound I on reduction in both C*c*P and APX. This would be consistent with the observation that the distal arginine is conserved in all peroxidases.

Overall Conclusions—Compound I formation is implicated as a common intermediate in many catalytic heme enzymes but, as we show in Scheme 1, there is more than one mechanism for its formation, and different heme enzymes use different preferred pathways. Compound I in P450s is highly unstable and has been difficult to capture even using fast spectroscopic methods; the corresponding intermediate has been yet more elusive in the NO synthases so that reliable crystal structures for Compound I intermediates in these enzymes have yet to emerge. Our structures, summarized in Scheme 2, show a consistent picture for the ferryl heme species across two different enzymes. In view of the mechanistic similarities that are a hallmark of heme enzyme chemistry, it is very likely that this snapshot of peroxidase structures represents a more general picture across the wider family and is thus likely to be relevant to the development of our understanding of other, less well characterized, catalytic heme enzymes.

Acknowledgments—We are grateful to Professor Grant Mauk (University of British Columbia) for the gift of the CcP expression vector, to Dr. X. Yang (University of Leicester) for assistance with the subcloning of CcP, Dr. Igor Efimov (University of Leicester) and Philip Raynor (University of Leicester) for assistance with synchrotron experiments, Dr. Antoine Royant (ESRF) for the help during data collection at ESRF, Ralf Flaig (Diamond Light Source) for flux measurements from DLS IO4, and Professor George Sheldrake (University of Göttingen) for help with SHELX.

Addendum—While this work was being written up for publication, a related study appeared (32) in which this 1.87 bond length in C*c*P has been reassessed. The structure reports an Fe–O distance of 1.73 Å for Compound I of C*c*P, which is longer than the distance (1.63 Å) reported here (the dose received in these experiments was approximately one-third more than the dose reported here) but still consistent with an unprotonated ferryl-oxy species.

REFERENCES

1. Valentine, J. S., Foote, C. S., Greenburg, A., and Liebman, J. F. (1995) *Active Oxygen in Biochemistry*, Chapman & Hall, London
2. Montellano, P. R. O. (2005) *Cytochrome P450: Structure, Mechanism and Biochemistry*, 3rd Ed., Kluwer Academic/Plenum, New York
3. Zhu, Y., and Silverman, R. B. (2008) *Biochemistry* **47,** 2231–2243
4. Dawson, J. H. (1988) *Science* **240,** 433–439
5. Dunford, H. B. (2010) *Peroxidases and Catalases: Biochemistry, Biophysics, Biotechnology and Physiology*, 2nd Ed., John Wiley & Sons, Inc., Chichester, UK
6. Karlin, K. D. (2010) *Nature* **463,** 168–169
7. Green, M. T. (2006) *J. Am. Chem. Soc.* **128,** 1902–1906
8. Berglund, G. I., Carlsson, G. H., Smith, A. T., Szöke, H., Henriksen, A., and Hajdu, J. (2002) *Nature* **417,** 463–468
9. Goodin, D. B., Davidson, M. G., Roe, J. A., Mauk, A. G., and Smith, M. (1991) *Biochemistry* **30,** 4953–4962
10. Metcalfe, C. L., Ott, M., Patel, N., Singh, K., Mistry, S. C., Goff, H. M., and Raven, E. L. (2004) *J. Am. Chem. Soc.* **126,** 16242–16248
11. Pipirou, Z., Bottrill, A. R., Svistunenko, D. A., Efimov, I., Basran, J., Mistry, S. C., Cooper, C. E., and Raven, E. L. (2007) *Biochemistry* **46,** 13269–13278
12. Metcalfe, C., Macdonald, I. K., Murphy, E. J., Brown, K. A., Raven, E. L., and Moody, P. C. (2008) *J. Biol. Chem.* **283,** 6193–6200

13. Sharp, K. H., Mewies, M., Moody, P. C., and Raven, E. L. (2003) *Nat. Struct. Biol.* **10,** 303–307
14. Evans, P. (2006) *Acta Crystallogr. D Biol. Crystallogr.* **62,** 72–82
15. Collaborative Computational Project Number 4 (1994) *Acta Crystallogr. D Biol. Crystallogr.* **50,** 760–763
16. Kabsch, W. (1993) *J. Appl. Crystallogr.* **26,** 795–800
17. Paithankar, K. S., and Garman, E. F. (2010) *Acta Crystallogr. D Biol. Crystallogr.* **66,** 381–388
18. Unno, M., Chen, H., Kusama, S., Shaik, S., and Ikeda-Saito, M. (2007) *J. Am. Chem. Soc.* **129,** 13394–13395
19. Murshudov, G. N., Vagin, A. A., and Dodson, E. J. (1997) *Acta Crystallogr. D Biol. Crystallogr.* **53,** 240–255
20. Finzel, B. C., Poulos, T. L., and Kraut, J. (1984) *J. Biol. Chem.* **259,** 13027–13036
21. Emsley, P., and Cowtan, K. (2004) *Acta Crystallogr. D Biol. Crystallogr.* **60,** 2126–2132
22. Sheldrick, G. (2008) *Acta Crystallogr. Sect. A* **64,** 112–122
23. Pond, A. E., Bruce, G. S., English, A. M., Sono, M., and Dawson, J. H. (1998) *Inorg. Chim. Acta* **275–276,** 250–255
24. Bonagura, C. A., Bhaskar, B., Shimizu, H., Li, H., Sundaramoorthy, M., McRee, D. E., Goodin, D. B., and Poulos, T. L. (2003) *Biochemistry* **42,** 5600–5608
25. Fülöp, V., Phizackerley, R. P., Soltis, S. M., Clifton, I. J., Wakatsuki, S., Erman, J., Hajdu, J., and Edwards, S. L. (1994) *Structure* **2,** 201–208
26. Edwards, S. L., Nguyen, H. X., Hamlin, R. C., and Kraut, J. (1987) *Biochemistry* **26,** 1503–1511
27. Lad, L., Mewies, M., and Raven, E. L. (2002) *Biochemistry* **41,** 13774–13781
28. Lad, L., Mewies, M., Basran, J., Scrutton, N. S., and Raven, E. L. (2002) *Eur. J. Biochem.* **269,** 3182–3192
29. Badyal, S. K., Metcalfe, C. L., Basran, J., Efimov, I., Moody, P. C., and Raven, E. L. (2008) *Biochemistry* **47,** 4403–4409
30. Newcomb, M., Halgrimson, J. A., Horner, J. H., Wasinger, E. C., Chen, L. X., and Sligar, S. G. (2008) *Proc. Natl. Acad. Sci. U.S.A.* **105,** 8179–8184
31. Patterson, W. R., and Poulos, T. L. (1995) *Biochemistry* **34,** 4331–4341
32. Meharenna, Y. T., Doukov, T., Li, H., Soltis, S. M., and Poulos, T. L. *Biochemistry* (2010) **49,** 2984–2986
33. Sivaraja, M., Goodin, D. B., Smith, M., and Hoffman, B. M. (1989) *Science* **245,** 738–740
34. Bursey, E. H., and Poulos, T. L. (2000) *Biochemistry* **39,** 7374–7379
35. Chance, M., Powers, L., Poulos, T., and Chance, B. (1986) *Biochemistry* **25,** 1266–1270
36. Davydov, R., Osborne, R. L., Kim, S. H., Dawson, J. H., and Hoffman, B. M. (2008) *Biochemistry* **47,** 5147–5155
37. Penner-Hahn, J. E., Eble, K. S., Mcmurry, T. J., Renner, M., Balch, A. L., Groves, J. T., Dawson, J. H., and Hodgson, K. O. (1986) *J. Am. Chem. Soc.* **108,** 7819–7825
38. Chance, B., Powers, L., Ching, Y., Poulos, T., Schonbaum, G. R., Yamazaki, I., and Paul, K. G. (1984) *Arch. Biochem. Biophys.* **235,** 596–611
39. Green, M. T., Dawson, J. H., and Gray, H. B. (2004) *Science* **304,** 1653–1656
40. Hersleth, H. P., and Andersson, K. K. (2010) *Biochim. Biophys. Acta*, in press
41. Penner-Hahn, J. E., McMurry, T. J., Renner, M., Latos-Grazynsky, L., Eble, K. S., Davis, I. M., Balch, A. L., Groves, J. T., Dawson, J. H., and Hodgson, K. O. (1983) *J. Biol. Chem.* **258,** 12761–12764
42. Behan, R. K., and Green, M. T. (2006) *J. Inorg. Biochem.* **100,** 448–459
43. Stone, K. L., Behan, R. K., and Green, M. T. (2005) *Proc. Natl. Acad. Sci. U.S.A.* **102,** 16563–16565
44. Behan, R. K., Hoffart, L. M., Stone, K. L., Krebs, C., and Green, M. T. (2006) *J. Am. Chem. Soc.* **128,** 11471–11474
45. Stone, K. L., Hoffart, L. M., Behan, R. K., Krebs, C., and Green, M. T. (2006) *J. Am. Chem. Soc.* **128,** 6147–6153
46. Green, M. T. (2009) *Curr. Opin. Chem. Biol.* **13,** 84–88
47. Chance, M., Powers, L., Kumar, C., and Chance, B. (1986) *Biochemistry* **25,** 1259–1265
48. Hersleth, H. P., Dalhus, B., Görbitz, C. H., and Andersson, K. K. (2002) *J. Biol. Inorg. Chem.* **7,** 299–304